This is the author-created version of the following work:

Webb, Jackie R., Santos, Isaac R., Tait, Douglas R., Sippo, James Z., Macdonald, Ben C.T., Robson, Barbara, Maher, Damien T., and UNSPECIFIED (2016) *Divergent drivers of carbon dioxide and methane dynamics in an agricultural coastal floodplain: post-flood hydrological and biological drivers.* Chemical Geology, 440 pp. 313-325.

Access to this file is available from:

https://researchonline.jcu.edu.au/58052/

Please refer to the original source for the final version of this work:

https://doi.org/10.1016/j.chemgeo.2016.07.025

Accepted Manuscript

Divergent drivers of carbon dioxide and methane dynamics in an agricultural coastal floodplain: post-flood hydrological and biological drivers

Jackie R. Webb[a,b*], Isaac R. Santos[a,b], Douglas R. Tait[a,b], James Z. Sippo[a,b], Ben C.T. Macdonald[c], Barbara Robson[d], Damien T. Maher[a,b]

[a]School of Environmental Science and Engineering, Southern Cross University, New South Wales, Australia

[b]National Marine Science Centre, Coffs Harbour, Southern Cross University, New South Wales, Australia

[c]CSIRO Agriculture, GPO Box 1666, Canberra, ACT 2601, Australia

[d]CSIRO Land and Water, GPO Box 1666, Canberra, ACT 2601, Australia

*Corresponding author Jackie Webb (j.webb.20@student.scu.edu.au). Ph: +61 468 730 184

Abstract

Many coastal floodplains have been artificially drained for agriculture, altering hydrological connectivity and the delivery of groundwater-derived solutes including carbon dioxide (CO_2) and methane (CH_4) to surface waters. Here, we investigated the drivers of CO_2 and CH_4 within the artificial drains of a coastal floodplain under sugarcane plantation and quantify the contribution of groundwater discharge to CO_2 and CH_4 dynamics over a flood (290 mm of rainfall). High temporal resolution, in situ observations of dissolved CO_2 and CH_4, carbon stable isotope for CH_4 ($\delta^{13}C$-CH_4), and the natural groundwater tracer radon (^{222}Rn) allowed us to quantify CO_2, CH_4 and groundwater dynamics during the rapid recession of a flood over a five day period. Extreme super-saturation of free CO_2 ($[CO_2^*]$) up to 2,951 μM (25,480% of atmospheric equilibrium) was driven by large groundwater input into the drains (maximum 87 cm day^{-1}), caused by a steep hydraulic head in the adjacent groundwater. Groundwater input sustained between 95-124% of the surface $[CO_2^*]$ flux during the flood recession by delivering high carbonate alkalinity groundwater (DIC = 10,533 μM, ~pH = 7.05) to acidic surface water (pH <4), consequently transforming all groundwater-derived DIC to $[CO_2^*]$. In contrast, groundwater was not a major direct driver of CH_4 contributing only 14% of total CH_4 fluxes. A progressive increase in CH_4 concentrations of up to ~2,400 nM day^{-1} occurred as a combination of increased substrate availability delivered by post-flood drainage water and longer residence times, which allowed for a biogenic CH_4 signal to develop. The progressive enrichment in $\delta^{13}C$-CH_4 values (-70‰ to -48‰) and increase in CH_4 concentrations (46-2,460 nM) support coupled production-oxidation, with concentrations and $\delta^{13}C$ values remaining higher (-47‰ and 2,798 nM) than pre-flood conditions (-55‰ and 534 nM) three weeks after the flood. Our findings demonstrate how separate processes can drive the aquatic CO_2 and CH_4 response to a flood

event in a drained coastal floodplain, and the key role groundwater had in post-flood $[CO_2^*]$ evasion to the atmosphere, but not CH_4.

1 Introduction

Floodplain ecosystems play an important role in carbon cycling at the terrestrial-aquatic interface, and have some of the highest global rates of primary production and carbon sequestration. Primary productivity in floodplain wetlands range from 205 to 2,438 g m^{-2} yr^{-1} (Mitsch et al., 1991; San-José et al., 2010), and carbon burial rates range from 57 to 921 g m^{-2} yr^{-1} (Hopkinson et al., 2012; Marín-Muñiz et al., 2014). However, understanding the processes driving carbon dioxide (CO_2) and methane (CH_4) cycling has proven difficult. Floodplains have variable hydrological regimes of discharge and inundation which can produce large carbon exports in the form of CO_2 and CH_4 outgassing and lateral aquatic discharge (Pulliam, 1993; Gatland et al., 2014). Carbon exports are often poorly quantified and not integrated into floodplain carbon budgets. Consequently, only a few estimates exist for carbon loss from floodplains (Pulliam, 1993; Gatland et al., 2014; Batson et al., 2015).

Changes in floodplain hydrology can produce feedback mechanisms in biogeochemical processes such as varying sediment and nutrient loads, alterations to aquatic metabolism, distribution in vegetation (Hamilton, 2010), and can also exert controls over greenhouse gas fluxes (Altor and Mitsch, 2008; Battin et al., 2008; Mitsch et al., 2010). Climate-driven changes in precipitation, conversion of wetlands to crops and intensification of artificial drainage can significantly alter the functioning of floodplain ecosystems (Hamilton, 2010; Schottler et al., 2014). Coastal floodplains in particular have been exposed to significant anthropogenic pressures such as agriculture and urban development. The average rate of wetland conversion to developed land has progressively increased to a current rate of about 1% yr^{-1} (Davidson, 2014).

The water quality issues associated with the drainage of modified coastal floodplains have been widely documented (Wilson et al., 1999; Johnston et al., 2003; Macdonald et al., 2004;

Macdonald et al., 2007). In pyritic coastal floodplains, changes in water table height due to drainage oxidises the underlying sediments which produces extreme acidification and deoxygenation events after floods (Wong et al., 2011). Under these conditions, extremely high post-flood CO_2 supersaturation has been recorded in floodplain drainage waters (Atkins et al., 2013; Gatland et al., 2014; Ruiz-Halpern 2015). These high pCO_2 values result in particularly high atmospheric fluxes. Climate models predict greater hydrological extremes, including more intense flood events, in regions of Australia where most of these modified coastal floodplains exist (Hughes, 2003). Therefore, there is a need to understand the consequences floods may have on fluvial CO_2 and CH_4 losses from these modified landscapes.

An abundance of labile organic matter can produce low oxygen conditions that generate high CO_2 and CH_4 concentrations in shallow floodplain groundwaters. Artificial drains can provide conduits for shallow groundwater to discharge into surface waters, effectively increasing hydrological connectivity (Johnston et al., 2005). Groundwater discharge can be an important source of CO_2 into surface small streams (Borges et al., 2015, Hotchkiss et al., 2015), however due to difficulties in constraining groundwater-surface water interactions, it is a pathway often neglected in aquatic carbon budgets (Macpherson, 2009). In coastal acid sulphate soil (CASS) floodplains, groundwater discharge can significantly alter the chemistry of drainage waters by contributing large quantities of reducible Fe, Mn, and SO_4^{-2} minerals, dissolved nutrients, and acid (Johnston et al., 2004; Burton et al., 2006; Santos et al., 2011; Jeffrey et al., 2016). This can affect the redox conditions of the surface water which combined with large quantities of labile organic matter may alter pathways and rates of carbon metabolism (Johnston et al., 2003; Wong et al., 2011). Understanding the influence groundwater discharge has on surface water carbon metabolism in these modified coastal floodplains may be critical for understanding CO_2 and CH_4 dynamics.

High resolution sampling is essential for capturing the temporal changes in carbon dynamics, which can undergo rapid transformations during and after a flood in floodplains. Here, we rely on high resolution observations of dissolved CH_4 concentrations and carbon stable isotope ratios (δ^{13}C-CH_4), dissolved CO_2, and radon (^{222}Rn, a natural groundwater tracer) following a flood in the drainage canals of an agricultural modified floodplain, to determine the main processes contributing to the post-flood response of CO_2 and CH_4. We attempt to resolve the contribution of floodwaters versus groundwater discharge to CO_2 and CH_4 exports. Our focus on quantifying the processes that enhance CO_2 and CH_4 concentrations after a flood contributes to quantifying the role of inland waters in the terrestrial carbon balance, where episodic events are often unaccounted for. We hypothesise that rapid drainage of flood waters will greatly enhance CO_2 and CH_4 concentrations, and that groundwater discharge will be primarily responsible for post-flood CO_2 and CH_4 dynamics in artificial drains.

2 Material and Methods

2.1 Study site

This study was undertaken in a hydrologically well constrained highly modified floodplain, where discharge, along with surface and groundwater levels are primarily controlled by a mechanical pump. The study site is a 100 ha sub-catchment situated within the low-lying Tweed River floodplain (28°17'1.69"S, 153°30'15.02"E) in Australia (Figure 1). The system represents a typical example of a natural wetland drained for agricultural development (in this case sugar cane cultivation). The Tweed floodplain consists of coastal acid sulphate soils containing high levels of iron sulphides (FeS_2) (Naylor et al., 1998). Sugarcane has been the dominant land use in the area for the last ~40 years. Prior to sugar cane cultivation the sub-

catchment had been modified wetland pasture since 1930, and was originally a low-lying freshwater wetland comprised of Melaleuca vegetation (Wilson, 1995).

Hydrology within the sub-catchment is greatly modified with a large network of shallow artificial drains (~12.9 km of drains within a 100 km^2 catchment), flap floodgates impeding tidal water infiltration, and an electric pump which controls surface and groundwater levels (Green et al., 2006). All drains within the catchment have shallow water depths, with the main drains having depths between 30 cm and 60 cm during baseline conditions. Smaller field drains are about 50 cm deep and usually only contain water after major rainfall. Two tidal creeks border the sub-catchment and a disconnected interception drain separates the site from neighbouring properties (Figure 1), making this a hydrologically isolated sub-catchment, except during floods (Smith et al., 2003). Catchment discharge is controlled by the automatic electric pump at the outlet of the sub-catchment (Figure 1), where pumping starts as water levels go above -453 mm Australian Height Datum (AHD) and stop when below -453 mm AHD (Green et al., 2006). As a result, groundwater levels are generally maintained at a relatively constant height of -0.5 m AHD (Smith et al., 2003), reducing groundwater seepage, except when significant rainfall events occur.

2.2 Sampling Strategy

Our experimental approach was to (1) monitor changes in CO_2 and CH_4 concentrations by undertaking high temporal resolution in situ CO_2, CH_4, $\delta^{13}C$-CH_4, and ^{222}Rn measurements within drainage waters from flood to return to pre-flood flow (2) construct a mass balance for groundwater using radon as tracer to quantify the contribution of groundwater to CO_2 and CH_4 dynamics post-flood, (3) constrain the major sources (groundwater and in-drain production) and sinks (aquatic export and gaseous evasion) of CO_2 and CH_4 to the surface waters of the catchment.

Firstly, discrete samples of dissolved CO_2, CH_4, $\delta^{13}C\text{-}CO_2$, $\delta^{13}C\text{-}CH_4$, ^{222}Rn, and water quality parameters were taken within the drain surface waters (Figure 1) both before, during, and after continuous monitoring. These discrete samples represent conditions described as pre-flood (1-3 weeks before flood), flood (period of inundation), and post-flood (1-3 weeks after flood recovery) and were taken from three different locations along the main drain (Figure 1). Water quality parameters were taken on site using a Hach®, HQ40d for pH, DO, and temperature, and a TROLL 9500 multiparameter sonde for conductivity. Six litre samples for surface water ^{222}Rn concentrations were collected in specially designed 8 L HDPE plastic bottles, leaving a headspace (Stringer and Burnett, 2004). A submersible Rule iL280 Amazon pump was used to sample water. Samples for dissolved CO_2 and CH_4 were collected in duplicate 200 mL opaque bottles with the submersible pump by filling the bottles from the bottom and overflowing approximately three times the volume. Samples were then treated with 200 μL of $HgCL_2$ and capped ensuring no headspace.

A 290 mm rain event over five days caused large portions of the floodplain to become inundated (up to 80 cm) between the 20th and 26th January 2015. During this time discrete samples were taken once a day between the 23rd and 25th to characterise concentrations during flood conditions. Field sampling was concentrated to flood waters rather than drains due to inundation of the catchment and carried out via the procedures described above.

High frequency continuous observations took place during the receding phase of the flood from 26th to 31st January 2015. A submersible pump was placed just above the bottom of the main drain, about 90 m upstream of the artificial pump, and delivered a constant stream of water through two showerhead-type gas equilibration devices (General Oceanics, Inc) following procedures described elsewhere (Maher et al., 2013; Webb et al, 2016). To maintain atmospheric pressure during air-water gas equilibration and avoid contamination with outside air, the first equilibrator was vented to a second equilibrator which was open to

the atmosphere. Sample air was pumped from the equilibrators at a rate of 1 L min^{-1} to three

gas analysers connected in series. Dissolved CH_4 and $\delta^{13}C$-CH_4 was measured on a cavity

ringdown spectroscopy (CRDS) analyser (Picarro G2201-i). An infrared gas analyser (LI-

840, LI-COR, Inc.) was used to measure dissolved CO_2 and a radon-in-air monitor (RAD7,

Durridge Co., Inc.) for radon. The equilibrated sample air was continuously pumped in a

closed air loop setup between the equilibration device and gas analyzers using an external air

pump (12 V DC micro diaphragm pump). The equilibration times for radon, CO_2 and CH_4

using this experimental setup are about 30 minutes, 5 minutes and 20 minutes respectively

(Santos et al., 2012, Webb et al., 2016).

Physiochemical water quality parameters were monitored during the time series. A calibrated

multi-parameter water quality logger (Hydrolab DS5X) was deployed in the drain next to the

pump to measure in situ temperature, conductivity, pH, and dissolved oxygen (DO). Depth

and velocity measurements were recorded using a Starflow (model 6529 G-512K) ultrasonic

Doppler flowmeter 100 m upstream of the artificial pump, positioned at the exit of a 76 cm

diameter pipe culvert. Discharge was calculated using the changing cross sectional area as a

function of depth within the pipe and the measured velocity (±2% error) at the time. Wind

data was obtained from an onsite weather station (R.M Young Wind Sentry Set) located

approximately 800 m downstream of the sampling site.

Groundwater samples for total alkalinity and dissolved CO_2 and CH_4 were collected from a

total of eight shallow wells. These groundwater locations were sampled both prior to and

after flood within the sub-catchment (Figure 1). Bores were dug using a hand auger, installed

with PVC pipes with 50-cm-long slotted screens, and sample water extracted via syringe after

purging the well water volume at least three times. Water table depths varied between 0.3-1.7

m below the surface during each sampling expedition. This allowed us to constrain any

heterogeneity in profile depths by obtaining an integrated endmember for the measured

groundwater-derived solutes (averages and errors are reported in Table 1). Sediments were taken for groundwater radon equilibration experiments from two different soil layers, the oxidised sulfuric zone and unconsolidated sulfidic zone which are typical profiles in the acid sulphate soils of the region (Johnston et al., 2009). In situ water quality parameters, including temperature, pH, dissolved oxygen, and conductivity were taken with a Hach®, HQ40d portable meter and a TROLL 9500 multiparameter sonde (for conductivity).

2.3 Analytical methods

2.3.1 Total alkalinity and DIC

Total alkalinity (TA) was determined by performing Gran titrations using a Metrohm Titrando automatic titrator. A Metrohm Electrode Plus was used for measuring pH during the titrations which was calibrated to Oakton National Bureau of Standards (NBS) of 4,7, and 10. Pre-standardized 0.01 mol L^{-1} HCl was used as the titrant. Replicates of each sample was run and the average of the two samples was used. The average uncertainty of duplicate TA measurements was 0.43% ± 0.73%. Total dissolved inorganic carbon (DIC) was calculated from the measured TA concentrations and field pH as determined in the Excel macro CO2SYS (version 25) (Pierrot et al., 2006). DIC calculations were run using the NBS pH scale and freshwater constants from Millero (1979) for K1 and K2 of carbonic acid.

2.3.2 Radon analysis

Discrete samples for radon analysis were connected to a radon-in-air monitor (RAD7, Durridge Co., Inc.) in a closed loop set-up for >2 h while equilibration was facilitated by continuous bubbling driven by the RAD7 internal air pump (Lee and Kim, 2006). Total volume of the sample in the bottle was ~ 6 L, leaving ~ 2 L of headspace for the equilibration to take place. Each sample volume was measured precisely with a graduated cylinder after

analysis. An average was taken of the >10 x 10 minute counting cycles after equilibration was reached between the water and air phase (equilibration time ~40 min, Lee and Kim, 2006) for each analysis. Radon concentrations were determined after accounting for radon lost through decay during the time from sample extraction to analysis. During the continuous measurement sampling phase, radon was measured in 10 minute cycles via the equilibrator setup described in section 2.2 (Burnett et al., 2001).

The groundwater radon endmember was characterised via six sediment incubations, following the sediment equilibration technique described in Corbett et al. (1998). Briefly, 1 kg sediment samples were obtained from two soil layers below the surface up to 1 m depth. Samples were only taken from this depth as shallow groundwater is the major interacting groundwater source with the surface water due to the presence of a 10 m thick layer of gel-like marine/estuarine clay that exists >1.5 m from the surface. This deeper sediment has a very low hydraulic conductivity (White et al., 2003), and acts as a confining layer between any deeper groundwater aquifers. Known volumes of radium-free tap water equilibrated with the atmosphere was added to the sediments and incubated for 21 days to allow for radon source (^{226}Ra decay) and sink (^{222}Rn decay) to reach steady state equilibrium. The radon concentration in the water was then measured on a RAD7 using procedures described above. The radon concentrations from each sediment incubation were averaged to provide an integrative groundwater radon endmember. This technique is a widely used approach for estimating the radon endmember in groundwater discharge studies (Burnett et al., 2007; Peterson et al 2008; Schmidt et al., 2010).

2.3.3 Groundwater discharge estimates

Groundwater discharge was estimated using a radon mass balance approach that estimates minimum possible groundwater discharge. The model is based on a radon mass balance

approach developed by Peterson et al. (2010) and modified by Santos and Eyre (2011), using the continuous radon measurements and taking into account ^{222}Rn sources from diffusion and radium (^{226}Ra) decay. Firstly, radon excess was calculated to estimate the surface water radon concentrations attributed to groundwater inputs:

$$^{222}Rn_{ex} = {}^{222}Rn - {}^{222}Rn_{min} \tag{1}$$

where ^{222}Rn$_{ex}$ (dpm m^{-3}) is the surface water radon concentrations that can be explained by groundwater inputs, ^{222}Rn (dpm m^{-3}) is the actual surface water radon concentrations measured during the time series, ^{222}Rn$_{min}$ is the minimum ^{222}Rn concentration in surface water observed when groundwater table is below the drain level (i.e. no groundwater input). This approach has been used previously (Peterson et al., 2008; Schmidt et al., 2010) and estimates maximum diffusion and ^{226}Ra because it assumes no groundwater discharge when radon reaches its minimum value. The minimum groundwater discharge was calculated by the proportion of surface water ^{222}Rn excess concentration to the average groundwater ^{222}Rn endmember concentration, multiplied by the discharge (Q, m^3 min^{-1}) when pump was on and the drain volume change (V_{diff}, m^3 min^{-1}) when pump was off:

Pump on $\qquad\qquad Q_{gw} = {}^{222}Rn_{ex}/{}^{222}Rn_{gw}*Q \tag{2}$

Pump off $\qquad\qquad Q_{gw} = {}^{222}Rn_{ex}/{}^{222}Rn_{gw}*V_{diff} \tag{3}$

Where Q_{gw} (m^3 min^{-1}) is the average groundwater discharge rate, ^{222}Rn$_{gw}$ (dpm m^{-3}) is the radon concentration in the groundwater endmember. Additionally, an upper limit to the groundwater flux can be calculated which takes into account the loss of ^{222}Rn via evasion and ^{222}Rn decay in transit downstream of where groundwater enters the surface water (Santos et al., 2011; Santos et al., 2014). Atmospheric evasion is often the largest form of ^{222}Rn loss from aquatic systems (Atkins et al., 2013; Sadat-Noori et al., 2015), however incorporating evasion can disproportionally overestimate groundwater flux in streams with high surface

area if ^{222}Rn concentrations are sampled at the location of groundwater entry (Peterson et al., 2010). Furthermore, it has been shown that evasion is not a major loss pathway for radon in channelized streams (Burnett et al., 2010). Here we opted for using the conservative minimum groundwater flux model as the similarity between the maximum surface ^{222}Rn concentrations and average groundwater ^{222}Rn concentrations suggested minor evasion and the short residence time of the system means minimal time for decay within the drains. Additional detail on this groundwater discharge model is described in De Weys et al. (2011), Peterson et al. (2010), and Sadat-Noori et al. (2015).

2.3.4 Carbon dioxide and methane analysis and fluxes

Dissolved CO_2 and CH_4 were prepared for analysis using a headspace technique (Gatland et al., 2014). Briefly, 50 mL of air free of CO_2 and CH_4 (Coregas "Zero Air") was added to each inverted bottle while simultaneously extracting 50 mL of sample water. After ~18 h of equilibration at room temperature (21°C) the headspace air was then extracted at the same rate as water was added back into the bottle, and put into gas tight 0.5 L Tedlar® film bags. Samples were diluted with 200 mL of zero air and analysed on a cavity ring down spectroscopy (CRDS) analyser (G2201-i Picarro Inc. Santa Clara, CA, USA) for concentrations and carbon stable isotope ratios. Each bag was run for 5-10 mins by connecting the bag to the inlet line which runs through a desiccant tube of $Mg(ClO_4)_2$ before entering the analyser. An average of the data output was recorded once concentrations stabilized within the analyser. The standard deviation between duplicate samples was on average 10% and 7% for CO_2 and CH_4 concentrations, and 0.28‰ and 0.61‰ for δ^{13}C-CO_2 and δ^{13}C-CH_4 values, respectively.

For the continuous monitoring, CH_4 concentrations and δ^{13}C-CH_4 values were measured at approximately one second intervals (later averaged to one minute) using a CRDS analyser

(Picarro G2201-*i*) on CH_4 isotope only mode (operational range 1.8-1500 ppm). The manufacturer guaranteed accuracy for CH_4 measured at concentrations >10 ppm is 50 ppb + 0.05% of reading for concentrations and <0.5‰ for $\delta^{13}C$-CH_4 values. CO_2 concentrations and $\delta^{13}C$-CO_2 values could not be measured on the CRDS as CO_2 concentrations exceeded the operating range of the analyser (>4000 ppm). CO_2 concentrations were instead measured every minute using an infrared gas analyser (IRGA) (LI-840A, LI-COR, USA) connected in series with the CRDS. Manufacturer accuracy is specified at <1.5% of reading within a measurement range of 0-20,000 ppm. The IRGA analyser was calibrated up to 20,000 ppm before deployment, and corrections were applied to measured CO_2 values >20,000 ppm using 20,000, 50,000 and 100,000 ppm standards that were analysed following the time series.

Aqueous CO_2 and CH_4 concentrations were then determined from Henry's law, using the measured equilibrated concentration obtained from the CRDS and IRGA (ppm), temperature and conductivity of the sample water, and atmospheric pressure. Concentrations were derived from the headspace fugacity of CO_2 and CH_4 as calculated according to Pierrot et al. (2009), assuming 100% humidity. Solubility coefficients for CO_2 and CH_4 were derived from Weiss (1974) and Yamamoto et al., (1976), respectively.

Air-water flux estimates of CO_2 and CH_4 (F, mmol m^{-2} d^{-1}) were calculated as follows:

$$F = k \propto (pC_{(water)} - pC_{(air)}) \tag{4}$$

where k is the gas transfer velocity (m d^{-1}), $\propto$ is the solubility coefficient of the respective gas, $pC_{(water)}$ is the partial pressure of CO_2 or CH_4 in water, and $pC_{(air)}$ is the partial pressure of CO_2 or CH_4 in the atmosphere. The k_{600} value was empirically derived from the O'Connor and Dobbins (1957) parameterisation using surface water velocity and depth:

$$k_{600} = 1.539w^{0.5}h^{-0.5} \tag{5}$$

where k_{600} is the gas transfer velocity (cm h^{-1}) for a gas with a Schmidt number of 600, w is the water velocity (cm s^{-1}) and h is the depth (m). The erratic nature of surface discharge at this site as controlled by the automatic pump meant that certain periods had zero detectable surface water velocity. To account for these periods, we applied a k_{600} value of 0.93 cm h^{-1} derived from Ho et al. (1997) to represent diffusion under zero flow conditions, allowing for the calculated evasion during these stagnant periods when the O'Connor and Dobbins (1958) reaeration equation breaks down due to zero velocity.

A total mass balance for CO_2 and CH_4 from the drains is balanced by the sum of the following parameters over the study period:

$$C_{total} = [C_{gw} + C_{drain}] - [C_f + C_Q] \tag{6}$$

Where C_{total} refers to the total flux of CO_2 or CH_4 generated from the aquatic system over the study period, C_{gw} is the total groundwater input, C_{drain} is the total in-drain production of CO_2 or CH_4, C_f is the total evasion flux from the drains, and C_Q is the total downstream export. Groundwater flux and in-drain production are inputs into the system and evasion and discharge are exports out of the system.

The groundwater discharge rate (Q_{gw}) determined by the radon mass balance was used as the final groundwater input in the mass balance. CO_2 and CH_4 derived groundwater fluxes were calculated by multiplying the average radon-derived groundwater input (Q_{gw}) by the CO_2 (GW-CO_2) or CH_4 (GW-CH_4) endmember concentration. The error provided for groundwater-derived CO_2 and CH_4 inputs was propagated using the standard error of both groundwater discharge (Table 2) and CO_2 and CH_4 endmember concentrations (Table 1). The minimum concentration was multiplied by the lower groundwater discharge and the maximum concentration was multiplied by the upper groundwater discharge. The difference between the average C_{gw} flux with the lower and upper C_{gw} flux range is the reported error.

Usually the free CO_2 [CO_2*] concentration, defined as aqueous $CO_2 + H_2CO_3$, in the groundwater is used as the endmember to calculate relative groundwater CO_2 contribution (Atkins et al., 2013). However, in this case we used the groundwater dissolved inorganic carbon (DIC) concentration derived from sampled alkalinity expressed as 'potential CO_2' for the endmember. This was warranted because of the large difference in pH between the drain water (pH 3-4) and groundwater (pH ~7.05) and therefore different speciation of the carbonate system with all DIC being in the form of [CO_2*] within the drains. For comparison, both the calculated [CO_2*] and DIC-CO_2 (i.e. potential CO_2) derived groundwater fluxes are shown and discussed in section 4.3.

Total CO_2 and CH_4 evasion (C_f) was calculated by taking the flux estimates calculated from O'Connor and Dobbins (1958) and Ho et al., (1997) multiplied by the changing drain surface area at each 10 minute interval. The cumulative fluxes were then calculated over the five days. Total aquatic CO_2 and CH_4 downstream export was calculated by the surface water discharge multiplied by dissolved CO_2 and CH_4 surface water concentration. Manufacturer specified instrumental errors were applied to the velocity recordings in the Starflow ultrasonic Doppler flowmeter and the CO_2 and CH_4 concentrations from the CRDS analyser to report final error propagated in export calculations. Having accounted for three of the mass balance terms, the total in-drain input (floodwater, sediment and aquatic metabolism) can be assumed as the 'missing' flux. Rearranging equation 6, C_{drain} can be determined:

$$C_{drain} = [C_f + C_Q] - C_{gw} \qquad (7)$$

Using this approach, the contribution of surface water and groundwater inputs feeding into the total drain CO_2 and CH_4 budget can be estimated. All other non-groundwater derived fluxes are assumed to result from production within the drains. Errors were propagated for in-drain calculations.

3 Results

A flood event occurred from 20th to 24th of January 2015 leading up to post-flood sampling after a 58 mm and 185 mm rainfall event, respectively (Figure 2). A total of 290 mm of rain fell and 9,794 m^3 of water discharged via the drains during the flood and sampling period. The oscillating surface water levels resulted from the automatic pump operating since the flood onset, and are not representative of natural drainage. Due to the catchment's enhanced drainage characteristics, the surface water hydrograph rises and falls rapidly in response to the rain event (Figure 2B). Peak discharge was reached 18 hours after the first 58 mm rainfall. The pumping switches off once water levels drop to 80 cm depth below the top of the drain surface. The height difference (cm) of groundwater and surface water suggests a steep hydraulic gradient where the rate of surface water discharge exceeds the rate of shallow groundwater flow throughout the soil (Figure 2B). During baseline conditions surface water and groundwater levels were similar. The rapid onset of the flood event followed by enhanced drainage shifted the floodplain hydrology from surface water excess to groundwater excess in a matter of 14 hours (Figure 2C). Surface water excess is defined by periods when the groundwater table is below the surface water level, such as during conditions when drains fill with floodwater faster than it takes for the groundwater table to rise. Groundwater excess is the opposite situation where the groundwater table is positioned above the surface water level, which occurs when drain waters are discharged faster than the groundwater discharge.

During the five day time series deployment, [CO$_2$] and CH$_4$ concentrations remained above equilibrium concentrations (which are ~12.9 µM and ~2.5 nM at in situ temperature, pH, conductivity and pressure) and spanned three orders of magnitude, 72-2,950 µM and 46-

2,460 nM respectively (Figure 3). During initial flood conditions [CO_2] and CH_4 concentrations average 284 ± 64 µM and 121 ± 53 nM respectively, similar to pre-flood conditions of ~193 µM and ~536 nM respectively (Table 1). The time series data was separated into four distinct phases highlighted in Figure 3 as flood (26/01/2015 16:00 to 23:00), groundwater excess (26/01/2015 23:00 to 27/01/2015 20:00), recovery (27/01/2015 20:00 to 29/01/2015 10:30), and baseline conditions (29/01/2015 10:30 to 31/01/2015 14:30).

Conductivity ranged from 670-5,015 µS cm^{-1} throughout the study. A significant increase from 728-3,468 µS cm^{-1} occurred during the groundwater excess phase before stabilising once the drain depth reached baseline levels. Surface water pH decreased substantially from 4.05-3.35 during the groundwater phase before also stabilising at ~3.2. Surface water temperatures ranged from 20.4 to 34.6°C with diurnal temperature changes spanning a much as 14°C between night and day. Dissolved oxygen saturation was highest during the day and lowest at night, with fluctuations between 15.3% and 98.4% during the first 2.5 days and 31% to 244% during the last 2.5 days.

Once floodwaters had receded and surface water became confined to the drainage canals, a five-fold and seven-fold increase in ^{222}Rn and CO_2 concentrations was observed respectively (Figure 3). This rapid increase in ^{222}Rn concentrations marked the start of the groundwater excess phase, where maximum ^{222}Rn concentrations of 150 dpm L^{-1} similar to the groundwater endmember average 146 ± 27 dpm L^{-1} of indicated drain water was derived purely from groundwater. In contrast to CO_2, CH_4 concentrations remained on a steady increase until the 30th January, yet δ^{13}C-CH_4 values decreased from -60‰ to -70‰ during the groundwater excess phase.

Radon levels remained high (30-100 dpm L^{-1}) during the recovery phase but decreased in a step wise fashion during the day and plateaued at night. Radon concentrations reached

baseline levels of 2-5 dpm L^{-1} after four days following the flood recession. CO_2

concentrations followed the same trend as ^{222}Rn, decreasing in a step wise fashion each day.

Yet CO_2 was not exclusively driven by groundwater as the ^{222}Rn trend may first indicate, but

also by photosynthesis during the day and respiration at night. This can be observed from the

sharp decrease in $[CO_2]$ from 2,835 to 1,900 µM in the groundwater surplus phase during the

day that is not replicated in ^{222}Rn levels. CH_4 continued to increase throughout the recovery

phase before it reached a maximum concentration of 2,459 nM six days post-flood. During

the baseline phase this was followed by a decrease from 2,459 to 275 nM. All daily peaks in

CH_4 appeared to occur between 9-11am following the minimum daily DO levels which

occurred at 7:30-8 am.

Table 1 shows the pre-flood baseline conditions, initial flood inundation, and post-flood

conditions for dissolved CO_2, CH_4, ^{222}Rn and water quality variables. Baseline concentrations

of $[CO_2]$ and CH_4 were on average 148 µM and 534 nM, respectively, which is 20- and 5-

fold lower than the peak concentrations observed during the flood recovery (Figure 3). Pre-

flood conditions represented a period following relatively low rainfall (133 mm in 80 days)

and was reflected by the high conductivity of drain water (43,335 µS cm^{-1}). The first flush of

the flood diluted CO_2, CH_4 and conductivity, increased ^{222}Rn to 36 dpm L^{-1}, and decreased

pH to 4.71 (Table 1). A 5.7‰ depletion in $\delta^{13}C$-CO_2 was observed from pre-flood to flood

conditions (from -9.3‰ to -14.9‰), whereas no significant change occurred in $\delta^{13}C$-CH_4

values. $\delta^{13}C$-CH_4 values increased from -53.0‰ to -47.1‰ between flood to post-flood

conditions. Average CO_2 and CH_4 concentrations were 223 ± 60 µM and $2,798 \pm 156$ nM

respectively during the post-flood period, which for CH_4 were the highest concentrations

observed during the entire study.

Table 2 shows the groundwater flux rate for the flood recovery period (continuous

monitoring) and the other terms associated with the radon mass balance calculations. The

aerial flux rate of groundwater flux, expressed as cm day^{-1} normalised to the drain area, is also provided. A total of $6,408 \pm 1,204$ m^3 groundwater was discharged into the drains over the five days of monitoring (uncertainty results from the standard error in the ^{222}Rn endmember concentrations; section 2.3.1). On average the groundwater flux rate for the entire period was 1,272 m^3 day^{-1}, which is equivalent to ~12 cm day^{-1}. The highest groundwater flux rate calculated was 8,138 m^3 day^{-1} (~ 85 cm day^{-1}) and occurred during the groundwater excess phase during flood recession. Over the five-day continuous monitoring period groundwater contributed an estimated $71 \pm 14\%$ of total surface water drain discharge.

4 Discussion

4.1 Drivers of CO$_2$ dynamics

The asynchronous relationship between CO_2 and CH_4 suggests different processes driving their production, consumption, and transport (Figure 3). Typically in natural floodplains, high CO_2 supersaturation in streams is sustained by wetland carbon inputs (Borges et al., 2015). In small tributaries groundwater becomes more important as a source of CO_2 (Hotchkiss et al., 2015). The contribution of groundwater may be enhanced in our study site by the lack of wetland coverage and artificial hydrology which creates a steep hydraulic head (Figure 3). The extreme CO_2 supersaturation was not sustained when groundwater input was negligible (average pCO$_2$ 3,055 μatm) in comparison to other small sub-tropical and tropical floodplain tributaries with wetland coverage sustaining higher pCO$_2$ values under non-flood conditions (7,500-12,000 μatm) (Abril et al., 2013; Gatland et al., 2014; Borges et al., 2015,). An important finding of this study is the extreme post-flood response observed for CO_2. The CO_2 concentrations observed in this study are four to eight-times higher than those reported in post-flood waters from other modified coastal floodplains (Atkins et al., 2013; Gatland et al., 2014; Ruiz-Halpern et al., 2015). These differences are likely related to the small catchment

and higher density of drains (12.4 km km^{-2}) in this study compared to other systems (0.2 to 3 km km^{-2}).

Although δ^{13}C-CO$_2$ values were not recorded during the time series, differences between the δ^{13}C-CO$_2$ values from the discrete samples and DIC samples taken during the time series reveal a distinct response to the flood event (Table 1). Discrete samples taken 5-6 weeks before time series deployment show that pre-flood δ^{13}C-CO$_2$ values (-9.3‰) were near atmospheric equilibrium (-8‰) (Fry, 2006). The flood event reduced CO$_2$ concentrations due to dilution, and a ~5.6‰ depletion in δ^{13}C-CO$_2$ values was observed (Table 1). The more enriched δ^{13}C-CO$_2$ values during pre-flood conditions are likely representative of high rates of in situ photosynthesis from aquatic plants within the relatively stagnant drain waters at the time. Additionally, methanogenesis would have contributed enriched δ^{13}C-CO$_2$ values to the CO$_2$ pool as methanogenesis produces an isotope separation factor of 40-60‰ between δ^{13}C-CO$_2$ and δ^{13}C-CH$_4$ (Whiticar, 1999). Both photosynthesis and methanogenesis are associated with a kinetic isotope effect and discriminate against the ^{13}CO$_2$, resulting in residual CO$_2$ that is enriched in ^{13}CO$_2$ (Whiticar, 1999; Fry, 2006). During flood conditions the main CO$_2$ source likely shifted to soil respiration, producing a more depleted δ^{13}C-CO$_2$ value of -14.9‰. This is similar to the average groundwater δ^{13}C-CO$_2$ value of -16.5 ± 1.0‰, where the source of groundwater-derived CO$_2$ would also have been largely from soil respiration. Furthermore, organic matter decomposition from sugarcane is likely contributing to the CO$_2$ pool within the floodwater, which also has distinct C$_4$ plant δ^{13}C values of -13‰ to -11‰ (Neves et al., 2015), similar to the observed floodwater δ^{13}C-CO$_2$ values (Table 1).

Groundwater discharge played an important role in contributing to the extreme supersaturation of drain CO$_2$ losses. When the water table was 20 cm to 65 cm below the soil surface, high ^{222}Rn and CO$_2$ concentrations were sustained (Figure 4), which coincided with the highest average groundwater discharge rate of 5,885 m^3 day^{-1} (Table 2). Under baseline

conditions the water table remained at or below the drain surface water level (-70 cm below surface). Figure 4 demonstrates how groundwater input traced by radon decreases substantially after the water table reaches 70 cm below the surface. Based on our groundwater samples which had near neutral pH (6.7-7.9), the depth of the unconsolidated sulfidic marine clay layer can be as high as 0.4 m below the surface. Due to the neutral pH of sampled groundwater, the DIC groundwater endmember was mostly in the form of bicarbonate (HCO_3^-) and not CO_2 (Millero, 1979). However, after large rainfall events the water table rises to the soil surface and groundwater spans across two distinct soil layers containing different geochemistry (Figure 5). Due to the major pH differences between the reduced and oxidised layer, the groundwater-derived [CO_2^*] endmember will be significantly higher in the oxidised sulfuric surface layer (pH <4.4). Considering that the fate of all groundwater-derived DIC being discharged is entering into acidic surface waters (pH<4.2, Figure 5), the groundwater-derived input of [CO_2^*] should be calculated based on the DIC endmember. As a result, the [CO_2^*] endmember (groundwater DIC = 10,533 μM) was six-fold greater than originally assumed (groundwater [CO_2] = 1,693 μM). This lead to a more realistic groundwater-derived [CO_2^*] input which contributes 99% of the total CO_2 surface budget during the groundwater excess stage (Figure 5), compared to only a 16% contribution assuming the endmember was 1,693 μM (Table 3).

During the recovery and baseline phase, groundwater remained the dominant source of excess CO_2 (Figure 5), however other processes were starting to drive much of the temporal variability. Drain diurnal metabolism became more pronounced as DO saturation fluctuated from 42% to 240% between night and day (Figure 3). This consequently decreased surface water CO_2 concentrations substantially during the day. The mass balance calculations also indicated that large CO_2 consumption was occurring (~24% of the CO_2 inputs were unaccounted for during baseline, Figure 5). Shallow agricultural drains can experience

extremely high metabolism due to high light and nutrients levels under warm conditions, resulting in large oscillations in DO saturation (Johnston, 2003; Santos and Eyre, 2011). More specifically to acid sulphate soil drains, the combination of low pH and oxygenated waters increases the bioavailability of organically complexed nutrients (Ahern et al., 2006), which are likely to be high after a flood.

4.2 Drivers of CH_4 dynamics

The factors controlling CH_4 dynamics in floodplain surface waters are complex. Several physical and chemical factors including conductivity, sulphate, oxygen, organic matter content, water table position, temperature dependence, and ecosystem primary productivity are commonly found to influence the extent of methanogenesis (Moore and Roulet, 1993; Whiting and Chanton, 1993; Purvaja and Ramesh, 2001; Yvon-Durocher et al., 2014). However, drained wetlands do not necessarily exhibit the same functional relationships between environmental conditions driving CH_4 flux in natural wetlands (Turetsky et al., 2014). In acid sulphate soil landscapes, the production of CH_4 may be limited by the oxidation/reduction state, availability of labile substrate, and the availability of alternative electron acceptors such as Fe, Mn, and SO_4^{2-} (Ponnamperuma, 1972; Dent, 1986; Jugsujinda et al., 1996). Some unique behaviours in surface CH_4 concentrations observed here reflect the apparent differences in the drivers of fluvial CH_4 concentrations in drained coastal wetlands.

The initial impact of the flood followed by groundwater excess appeared to reduce CH_4 concentrations to pre-flood concentrations rather than increase them. Typically CH_4 production is enhanced under high water table conditions (Bubier, 1995) which has been reported in other agricultural catchments with drainage ditches (Luan and Wu, 2015). However, in our study CH_4 production within the surface waters appeared to be hindered by higher groundwater levels and instead concentrations increased when the water table

decreased to below -65 cm (Figure 4). When groundwater discharge was high, substantial quantities of H_2SO_4 and Fe oxides would likely have been released into the surface water (Sammut et al., 1996; Wilson et al., 1999; Burton et al., 2006). It is well known that sulfate reducing microbes compete with methanogens for organic substrates and H_2, preferentially inhibiting methanogenesis (Gauci et al., 2000; Dowrick et al., 2006; Baldwin and Mitchell, 2012). The depleted $\delta^{13}C$-CH_4 values (-69‰ to -63‰) during the groundwater excess stage are in the range of the groundwater CH_4 endmember (-66.6 ± 4.9‰), suggesting that groundwater may be contributing the majority of surface water CH_4. However, mass balance calculations indicate that groundwater contributed 57% of the surface water CH_4 budget during this phase (Figure 5). Rapid transport of surface water CH_4 derived from the floodwater likely explains the other half of the CH_4 budget during this stage. The more depleted isotope values are indicative of limited CH_4 oxidation, which is likely due to the high water discharge (i.e. short residence time) transporting freshly produced CH_4 rapidly out of the system. The $\delta^{13}C$-CH_4 values also suggest that the original source of CH_4 is produced via the fermentation pathway (between -65‰ to -50‰), which is dominant in freshwater environments (Whiticar and Faber, 1986).

Once the water table gradually lowered and groundwater discharge decreased, CH_4 concentrations and $\delta^{13}C$-CH_4 values increased simultaneously over four days and a strong diurnal control over CH_4 concentration resumed (Figure 3). Methane oxidation, a microbial process which consequently enriches the residual CH_4 in the heavier isotope (Whiticar, 1999), often increases with higher CH_4 concentrations (and consequently production) (Boon and Lee, 1997; Shelley et al., 2014). The drain sediment at the study site, classified as monosulfidic black ooze, likely supports the coupling between methanogens and methanotrophs (Figure 5). Redox conditions within the monosulfides at the bottom of drains and the boundary between the sediment-water interface have demonstrated a rapid shift from

oxic (Eh 100-150 mV) to anoxic (-50-100 mV) in a matter of ~10 cm (Smith and Melville, 2004). Complex interactions between CH_4 and other electron acceptors such as iron oxides and sulfate are likely occurring in near-surface monosulfidic black oozes that are unique to acid sulphate soil drains (Smith and Melville, 2004), and should be investigated in detail in future research.

Physical processes controlled by the decrease in discharge are likely contributing to the overall increase in CH_4 concentrations. The increasing water residence time as a result of less frequent pumping (Figure 2) could lead to a greater accumulation of CH_4 in the water column, while allowing for CH_4 oxidation to influence $\delta^{13}C$-CH_4 values. Some interesting diel trends in CH_4 dynamics can also be observed. Figure 6A shows 24 h trends in CH_4 concentrations during the five days of flood recovery. There is a clear trend of increasing CH_4 concentrations between 9 pm to 10-12 am, indicating a dominance of production over oxidation, before decreasing during the light hours of 12 pm to 5-8 pm (Figure 6). Such diurnal trends become more distinct over time until the maximum oscillation in CH_4 occurred on day five of the time series where concentrations dropped from 2,459 nM to 280 nM during the oxidation period (Figure 6A). Diel CH_4 oscillations seem to be related to the dissolved oxygen levels produced in the water column, however a time lag exists in the oxygen diffusion into the sediments. Figure 6B illustrates the time lag between water column CH_4 concentrations in response to DO saturation within the overlying water through diel hysteresis loops. Cycling between aerobic methane oxidation during the day and anaerobic methane production during the night has been shown to drive diurnal oscillations in surface water CH_4 concentrations and $\delta^{13}C$-CH_4 values (King et al., 1990; Maher et al., 2013; Maher et al., 2015). In this case, the extent of CH_4 production and oxidation, the net result of measured concentrations and $\delta^{13}C$-CH_4 values, is likely controlled by the surface water residence time which increases as flood waters recede (Figure 2). Drain samples taken the 5-6

weeks after intensive sampling period showed a δ^{13}C-CH$_4$ value of -47.1‰ (Table 1), indicating the growing importance of methane oxidation as water residence time increases. Furthermore, high average CH$_4$ concentrations of 2,798 ± 156 nM indicates that the flood had a sustained effect on CH$_4$ production, likely via increased substrate availability at the sediment surface (Figure 5).

4.3 Mass balance

The contribution of fluxes from various aquatic pathways were determined and partitioned into the different phases (Table 3, Figure 5). Evasion remained the largest loss term for both CO$_2$ and CH$_4$ during flood to baseline conditions (Figure 5). CO$_2$ and CH$_4$ evasion spanned 1-2 orders of magnitude greater than export loss via controlled pumping across all phases (Table 3). The flood, groundwater excess, and recovery phases contributed 96% of the total CO$_2$ evasion. The large area occupied by surface water inundation accounted for the largest CO$_2$ flux during the flood phase, whereas the high partial pressures and shallow conditions contributed to the high evasion rates observed for the remaining phases. In contrast, CH$_4$ evasion between the flood, recovery and baseline phases remained consistent and contributed 23-40% of total CH$_4$ evasion over the time series, whereas CH$_4$ evasion during the groundwater excess phase contributed only 11% to total evasion (Table 3).

Table 3 shows the average groundwater flux estimates applied to two different endmember scenarios for CO$_2$ (total DIC and [CO$_2^*$]). The [CO$_2$*] groundwater endmember flux is the traditional approach used to estimate groundwater derived CO$_2$ fluxes within an aquatic system (Atkins et al., 2013; Perkins et al., 2015). Here using [CO$_2$*] results in a relatively small groundwater contribution (~16%) to the total surface CO$_2$ budget during the groundwater excess phase. This is a severe underestimation in such a system where the pH difference between the surface water and groundwater easily transforms all DIC into [CO$_2$*].

The groundwater-DIC concentration was six times higher than $[CO_2^*]$, and is a measure of 'potential CO_2' that accounts for the carbonate equilibrium shift that would be occurring following groundwater seepage into the acidic drains. Using this endmember, groundwater contribution to the total CO_2 flux during the groundwater surplus phase becomes 99% (Figure 5). This revised $[CO_2^*]$ endmember calculation is more in agreement with the seven-fold increase in surface water $[CO_2^*]$ concentrations that occurred with a five-fold increase in surface ^{222}Rn during the groundwater excess phase. This highlights the need to account for carbon transformations as groundwater mixes with surface waters.

In contrast to CO_2, groundwater-derived CH_4 was a very minor component of the total surface CH_4 budget (14%). The largest contribution of groundwater to the surface CH_4 budget was 57% during the groundwater excess phase (Figure 5), however this phase played a minor role in total CH_4 fluxes over the entire study (~12%). This supports the hypothesis that shallow drain sediments or hyporheic production of CH_4 play an important role in driving the total CH_4 flux to the atmosphere. Groundwater had relatively low CH_4 concentrations of 548 ± 185 nM compared to peak surface water concentrations which were an order of magnitude greater. Groundwater usually has a higher CH_4 concentration than corresponding surface water, however reported concentrations are highly variable (56-53,000 nM) (Cable et al., 1996; Santos et al., 2009; O'Reilly et al., 2015; Sadat-Noori et al., 2015b). High concentrations of reduced metabolites including H_2S and FeS_2 are likely to be present (Rosicky et al., 2004) which may inhibit methanogenesis (Khan and Trottier, 1978).

After quantifying the fluxes and exports of $[CO_2^*]$ and CH_4, our results show that the magnitude and variability of $[CO_2^*]$ and CH_4 response to flood events can be greatly perturbated within extensively drained coastal floodplains. The most significant changes in $[CO_2^*]$ and CH_4 dynamics were caused by groundwater discharge and in-drain metabolism which occurred over approximately 10 hours and could only have been captured using the

high resolution continuous instrumentation used in this study. Similar setups have been used to continuously monitor $[CO_2^*]$ and CH_4 in aquatic environments, and have revealed distinct changes over short lived timescales caused by processes such as tidal pumping, porewater exchange, and diel metabolic cycles (Maher et al., 2013; Call et al., 2015; Maher et al., 2015; Gatland et al., 2014; Looman et al., 2016). However, the magnitude of change in surface water $[CO_2^*]$ concentrations captured in this study, spanning 2,700 μM (71,000 μatm) far exceeds that observed in the reported studies over half-day time scales. Although larger fluctuations have been observed for CH_4 concentrations in other systems (Sadat-Noori et al., 2015b), the CH_4 concentration fluctuations caused by diurnal DO oscillations reported here (2,200 nM) were larger than the typical range reported in other recent studies (Maher et al., 2015). Such findings highlight the profound effect flood events can have on fluvial $[CO_2^*]$ and CH_4 emissions from drained coastal floodplains. Considering that the Eastern Australia coastal region is subject to frequent large rainfall events (Alexander and Arblaster, 2009) that flood small catchments, the impact fluvial CO_2 and CH_4 emissions have on ecosystem carbon balances should be further investigated and quantified.

5 Conclusion

Through high resolution, continuous monitoring, major shifts in CO_2 and CH_4 dynamics were captured during a receding flood, revealing important controls in the CO_2 and CH_4 flood response within artificial coastal floodplain drains. The major drivers of CO_2 and CH_4 dynamics in the surface water budget operated on different processes and temporal scales. Methane sources were dominated by a combination of physical transport and biological processes in the surface water, and groundwater was a relatively minor source of CH_4. Post-flood conditions appeared to enhance large diurnal oscillations in CH_4 concentrations by up

to ten-fold, despite oxygen enriched surface waters during the day. Groundwater input sustained high surface water $[CO_2^*]$ flux by delivering high carbonate alkalinity groundwater to acidic surface water which transformed all groundwater-derived DIC to $[CO_2^*]$. Such findings on the groundwater-surface water CO_2 relationship highlights a new paradigm on the quantification of groundwater derived CO_2 flux into acidic surface waters. Considering the sensitivity of CO_2 to pH, we suggest that groundwater and surface water pH be taken into account when calculating groundwater-derived CO_2 input into aquatic systems. Where the pH is profoundly different between the surface water and groundwater, the groundwater DIC pool should be used to provide a more accurate measure of groundwater inputs of $[CO_2^*]$ in acidic surface waters.

6 Acknowledgements

7 References

Abril, G., Martinez, J.-M., Artigas, L. F., Moreira-Turcq, P., Benedetti, M. F., Vidal, L., Meziane, T., Kim, J.-H., Bernardes, M. C., Savoye, N., Deborde, J., Souza, E. L., Alberic, P., Landim de Souza, M. F., and Roland, F., 2013. Amazon River carbon dioxide outgassing fuelled by wetlands. Nature, 505(7483): 395-398.

Ahern, K.S., Udy, J.W., Pointon, S.M., 2006. Investigating the potential for groundwater from different vegetation, soil and landuses to stimulate blooms of the cyanobacterium, Lyngbya majuscula, in coastal waters. Marine and Freshwater Research, 57(2): 177-186.

Alexander, L.V., Arblaster, J.M., 2009. Assessing trends in observed and modelled climate extremes over Australia in relation to future projections. International Journal of Climatology, 29(3): 417-435.

Altor, A.E., Mitsch, W.J., 2008. Pulsing hydrology, methane emissions and carbon dioxide fluxes in created marshes: a 2-year ecosystem study. Wetlands, 28(2): 423-438.

Atkins, M.L., Santos, I.R., Ruiz-Halpern, S., Maher, D.T., 2013. Carbon dioxide dynamics driven by groundwater discharge in a coastal floodplain creek. Journal of Hydrology, 493(0): 30-42.

Baldwin, D.S., Mitchell, A., 2012. Impact of sulfate pollution on anaerobic biogeochemical cycles in a wetland sediment. Water Research, 46(4): 965-974.

Battin, T.J. Kaplan, L. A., Findlay, S., Hopkinson, C. S., Marti, E., Packman, A. I., Newbold, J. D., Sabater, F., 2008. Biophysical controls on organic carbon fluxes in fluvial networks. Nature Geoscience, 1(2): 95-100.

Boon, P.I., Lee, K., 1997. Methane oxidation in sediments of a floodplain wetland in south-eastern Australia. Letters in Applied Microbiology, 25(2): 138-142.

Borges, A.V., Abril, G.; Darchambeau, F.; Teodoru, C. R.; Deborde, J.; Vidal, L. O.; Lambert, T.; Bouillon, S., 2015. Divergent biophysical controls of aquatic CO_2 and CH_4 in the World's two largest rivers. Scientific Reports, 5: 15614.

Bubier, J.L., 1995. The relationship of vegetation to methane emission and hydrochemical gradients in northern peatlands. Journal of Ecology: 403-420.

Burnett, W.C., Santos, I.R., Weinstein, Y., Swarzenski, P.W., Herut, B., 2007. Remaining uncertainties in the use of Rn-222 as a quantitative tracer of submarine groundwater discharge, in: Sanford, W., Langevin, C., Polemio, M., Povinec, P. (Eds.), A new focus on groundwater-seawater interactions. IAHS Publication No 312, Perugia, Italy, pp. 109-118.

Burton, E.D., Bush, R.T., Sullivan, L.A., 2006. Sedimentary iron geochemistry in acidic waterways associated with coastal lowland acid sulfate soils. Geochimica et Cosmochimica Acta, 70(22): 5455-5468.

Cable, J.E., Burnett, W.C., Chanton, J.P., Weatherly, G.L., 1996. Estimating groundwater discharge into the northeastern Gulf of Mexico using radon-222. Earth and Planetary Science Letters, 144(3–4): 591-604.

Call, M. Maher, D. T.; Santos, I. R.; Ruiz-Halpern, S.; Mangion, P.; Sanders, C. J.; Erler, D. V.; Oakes, J. M.; Rosentreter, J.; Murray, R.; Eyre, B. D., 2015. Spatial and temporal variability of carbon dioxide and methane fluxes over semi-diurnal and spring–neap–spring timescales in a mangrove creek. Geochimica et Cosmochimica Acta, 150: 211-225.

Corbett, D., Burnett, W., Cable, P., Clark, S., 1998. A multiple approach to the determination of radon fluxes from sediments. Journal of Radioanalytical and Nuclear Chemistry, 236(1-2): 247-253.

Davidson, N.C., 2014. How much wetland has the world lost? Long-term and recent trends in global wetland area. Marine and Freshwater Research, 65(10): 934-941.

Dent, D., Pons, L., 1995. A world perspective on acid sulphate soils. Geoderma, 67(3): 263-276.

Devol, A.H., Richey, J.E., Clark, W.A., King, S.L., Martinelli, L.A., 1988. Methane emissions to the troposphere from the Amazon floodplain. Journal of Geophysical Research: Atmospheres, 93(D2): 1583-1592.

De Weys, J., Santos, I.R., Eyre, B.D., 2011. Linking Groundwater Discharge to Severe Estuarine Acidification during a Flood in a Modified Wetland. Environmental Science & Technology, 45(8): 3310-3316.

Dowrick, D.J., Freeman, C., Lock, M.A., Reynolds, B., 2006. Sulphate reduction and the suppression of peatland methane emissions following summer drought. Geoderma, 132(3–4): 384-390.

Fry, B. (2006), Stable Isotope Ecology, Springer, New York, United States of America, pp 295.

Gauci, V., Dise, N., Fowler, D., 2000. Controls on suppression of methane flux from a peat bog subjected to simulated acid rain sulfate deposition. Global Biogeochemical Cycles, 16(1): 10.1029.

Gatland, J., Santos, I., Maher, D., Duncan, T., Erler, D., 2014. Carbon dioxide and methane emissions from an artificially drained coastal wetland during a flood: Implications for wetland global warming potential. Journal of Geophysical Research: Biogeosciences, 119(8): 1698-1716.

Green, R., Macdonald, B.C.T., Melville, M.D., Waite, T.D., 2006. Hydrochemistry of episodic drainage waters discharged from an acid sulfate soil affected catchment. Journal of Hydrology, 325(1–4): 356-375.

Hamilton, S.K., 2010. Biogeochemical implications of climate change for tropical rivers and floodplains, Global Change and River Ecosystems—Implications for Structure, Function and Ecosystem Services. Springer, pp. 19-35.

Ho, D.T., Bliven, L.F., Wanninkhof, R.I.K., Schlosser, P., 1997. The effect of rain on air-water gas exchange. Tellus B, 49(2): 149-158.

Hopkinson, C.S., Cai, W.-J., Hu, X., 2012. Carbon sequestration in wetland dominated coastal systems; a global sink of rapidly diminishing magnitude. Current Opinion in Environmental Sustainability, 4(2): 186-194.

Hotchkiss, E. Hall Jr, R., Sponseller, R., Butman, D., Klaminder, J., Laudon, H., Rosvall, M., Karlsson, J., 2015. Sources of and processes controlling CO_2 emissions change with the size of streams and rivers. Nature Geoscience, 8(9): 696-699.

Hughes, L., 2003. Climate change and Australia: Trends, projections and impacts. Austral Ecology, 28(4): 423-443.

Jeffrey, L.C., Maher, D.T., Santos, I.R., McMahon, A., Tait, D.R., 2016. Groundwater, Acid and Carbon Dioxide Dynamics Along a Coastal Wetland, Lake and Estuary Continuum. Estuaries and Coasts: 1-20.

Johnston, S.G., Kroon, F., Slavich, P.G., Cibilic, A., Bruce, A., 2003. Restoring the balance: Guidelines for managing floodgates and drainage systems on coastal floodplains. NSW Agriculture, Wollongbar, NSW. ISBN: 0734715188

Johnston, S.G., Slavich, P.G., Hirst, P., 2004. The effects of a weir on reducing acid flux from a drained coastal acid sulphate soil backswamp. Agricultural Water Management, 69(1): 43-67.

Johnston, S.G., Slavich, P.G., Hirst, P., 2005. Opening floodgates in coastal floodplain drains: effects on tidal forcing and lateral transport of solutes in adjacent groundwater. Agricultural Water Management, 74(1): 23-46.

Johnston, S.G., Hirst, P., Slavich, P.G., Bush, R.T., Aaso, T., 2009. Saturated hydraulic conductivity of sulfuric horizons in coastal floodplain acid sulfate soils: Variability and implications. Geoderma, 151(3–4): 387-394.

Jugsujinda, A., Delaune, R.D., Lindau, C.W., Sulaeman, E., Pezeshki, S.R., 1996. Factors controlling carbon dioxide and methane production in acid sulfate soils. Water, Air, and Soil Pollution, 87(1-4): 345-355.

Khan, A., Trottier, T., 1978. Effect of sulfur-containing compounds on anaerobic degradation of cellulose to methane by mixed cultures obtained from sewage sludge. Applied and Environmental Microbiology, 35(6): 1027-1034.

King, G.M., Roslev, P., Skovgaard, H., 1990. Distribution and rate of methane oxidation in sediments of the Florida Everglades. Applied and Environmental Microbiology, 56(9): 2902-2911.

Lee, J.-M., Kim, G., 2006. A simple and rapid method for analyzing radon in coastal and ground waters using a radon-in-air monitor. Journal of Environmental Radioactivity, 89(3): 219-228.

Luan, J., Wu, J., 2015. Long-term agricultural drainage stimulates CH_4 emissions from ditches through increased substrate availability in a boreal peatland. Agriculture, Ecosystems & Environment, 214: 68-77.

Macdonald, B.C.T. Smith, J., Keene, A. F., Tunks, M., Kinsela, A., White, I., 2004. Impacts of runoff from sulfuric soils on sediment chemistry in an estuarine lake. Science of The Total Environment, 329(1–3): 115-130.

Macdonald, B.C.T. White, I., Åström, M. E., Keene, A. F., Melville, M. D., Reynolds, J. K., 2007. Discharge of weathering products from acid sulfate soils after a rainfall event, Tweed River, eastern Australia. Applied Geochemistry, 22(12): 2695-2705.

Macpherson, G.L., 2009. CO_2 distribution in groundwater and the impact of groundwater extraction on the global C cycle. Chemical Geology, 264(1–4): 328-336.

Maher, D.T. Santos, I. R., Leuven, J. R., Oakes, J. M., Erler, D. V., Carvalho, M. C., Eyre, B. D., 2013. Novel use of cavity ring-down spectroscopy to investigate aquatic carbon cycling from microbial to ecosystem scales. Environmental Science & Technology, 47(22): 12938-12945.

Maher, D.T., Cowley, K., Santos, I.R., Macklin, P., Eyre, B.D., 2015. Methane and carbon dioxide dynamics in a subtropical estuary over a diel cycle: Insights from automated in situ radioactive and stable isotope measurements. Marine Chemistry, 168(0): 69-79.

Marín-Muñiz, J.L., Hernández, M.E., Moreno-Casasola, P., 2014. Comparing soil carbon sequestration in coastal freshwater wetlands with various geomorphic features and plant communities in Veracruz, Mexico. Plant and Soil, 378(1-2): 189-203.

Millero, F.J., 1979. The thermodynamics of the carbonate system in seawater. Geochimica et Cosmochimica Acta, 43(10): 1651-1661.

Mitsch, W. Nahlik, A., Wolski, P., Bernal, B., Zhang, L., Ramberg, L., 2010. Tropical wetlands: seasonal hydrologic pulsing, carbon sequestration, and methane emissions. Wetlands Ecology and Management, 18(5): 573-586.

Moore, T., Roulet, N., 1993. Methane flux: Water table relations in northern wetlands. Geophysical Research Letters, 20(7): 587-590.

Naylor, S.D., Chapman, G.A., Atkinson, G., Murphy, C.L., Tulau, M.J., Flewin, T.C., Milford, H.B., and Morand, D.T., 1998. Guidelines for the Use of Acid Sulphate soil Risk Maps. 2nd edition. DLWC.

Neves, L.A. Sarmanho, G. F., Cunha, V. S., Daroda, R. J., Aranda, D. A., Eberlin, M. N., Fasciotti, M., 2015. The carbon isotopic (C-13/C-12) signature of sugarcane bioethanol: certifying the major source of renewable fuel from Brazil. Analytical Methods, 7(11): 4780-4785.

O'Connor, D.J., Dobbins, W.E., 1958. Mechanism of reaeration in natural streams. Transactions of the American Society of Civil Engineers, 123(1): 641-666.

O'Reilly, C., Santos, I.R., Cyronak, T., McMahon, A., Maher, D.T., 2015. Nitrous oxide and methane dynamics in a coral reef lagoon driven by pore water exchange: Insights from automated high-frequency observations. Geophysical Research Letters, 42(8): 2885-2892.

Peterson, R.N. Burnett, W.C., Taniguchi, M., Chen, J., Santos, I. R., Ishitobi, T., 2008. Radon and radium isotope assessment of submarine groundwater discharge in the Yellow River delta, China. Journal of Geophysical Research: Oceans (1978–2012), 113(C9).

Peterson, R.N., Santos, I.R., Burnett, W.C., 2010. Evaluating groundwater discharge to tidal rivers based on a Rn-222 time-series approach. Estuarine, Coastal and Shelf Science, 86(2): 165-178.

Perkins, A.K., Santos, I.R., Sadat-Noori, M., Gatland, J.R., Maher, D.T., 2015. Groundwater seepage as a driver of CO_2 evasion in a coastal lake (Lake Ainsworth, NSW, Australia). Environmental Earth Sciences, 74(1): 779-792.

Pierrot, D., Lewis, E., Wallace, D., 2006. MS Excel program developed for CO_2 system calculations. ORNL/CDIAC-105a. Carbon Dioxide Information Analysis Center, Oak Ridge National Laboratory, US Department of Energy, Oak Ridge, Tennessee.

Pierrot, D. Neill, C., Sullivan, K., Castle, R., Wanninkhof, R., Lüger, H., Johannessen, T., Olsen, A., Feely, R.A., Cosca, C. E., 2009. Recommendations for autonomous underway pCO$_2$ measuring systems and data-reduction routines. Deep Sea Research Part II: Topical Studies in Oceanography, 56(8–10): 512-522.

Ponnamperuma, F., 1972. The chemistry of submerged soils. Academic Press NY and London.

Pulliam, W.M., 1993. Carbon Dioxide and Methane Exports from a Southeastern Floodplain Swamp. Ecological Monographs, 63(1): 29-53.

Purvaja, R., Ramesh, R., 2001. Natural and Anthropogenic Methane Emission from Coastal Wetlands of South India. Environmental Management, 27(4): 547-557.

Rosicky, M.A., Sullivan, L.A., Slavich, P.G., Hughes, M., 2004. Soil properties in and around acid sulfate soil scalds in the coastal floodplains of New South Wales, Australia. Soil Research, 42(6): 595-602.

Ruiz-Halpern, S., Maher, D.T., Santos, I.R., Eyre, B.D., 2015. High CO_2 evasion during floods in an Australian subtropical estuary downstream from a modified acidic floodplain wetland. Limnology and Oceanography, 60(1): 42-56.

Sadat-Noori, M., Santos, I.R., Sanders, C.J., Sanders, L.M., Maher, D.T., 2015a. Groundwater discharge into an estuary using spatially distributed radon time series and radium isotopes. Journal of Hydrology, 528: 703-719.

Sadat-Noori, M., Maher, D., Santos, I., 2015b. Groundwater Discharge as a Source of Dissolved Carbon and Greenhouse Gases in a Subtropical Estuary. Estuaries and Coasts: 1-18.

Sammut, J., White, I., Melville, M., 1996. Acidification of an estuarine tributary in eastern Australia due to drainage of acid sulfate soils. Marine and Freshwater Research, 47(5): 669-684.

San-José, J., Montes, R., Mazorra, M.A., Ruiz, E.A., Matute, N., 2010. Patterns and carbon accumulation in the inland water-land palm ecotone (morichal) across the Orinoco lowlands, South America. Plant Ecology, 206(2): 361-374.

Santos, I.R., Burnett, W.C., Dittmar, T., Suryaputra, I.G.N.A., Chanton, J., 2009. Tidal pumping drives nutrient and dissolved organic matter dynamics in a Gulf of Mexico subterranean estuary. Geochimica et Cosmochimica Acta, 73(5): 1325-1339.

Santos, I.R., Eyre, B.D., 2011. Radon tracing of groundwater discharge into an Australian estuary surrounded by coastal acid sulphate soils. Journal of Hydrology, 396(3–4): 246-257.

Santos, I.R., Maher, D.T., Eyre, B.D., 2012. Coupling Automated Radon and Carbon Dioxide Measurements in Coastal Waters. Environmental Science & Technology, 46(14): 7685-7691.

Santos, I.R., Bryan, K.R., Pilditch, C.A., Tait, D.R., 2014. Influence of porewater exchange on nutrient dynamics in two New Zealand estuarine intertidal flats. Marine Chemistry, 167: 57-70.

Schottler, S.P. Ulrich, J., Belmont, P., Moore, R., Lauer, J.W., Engstrom, D.R., Almendinger, J.E., 2014. Twentieth century agricultural drainage creates more erosive rivers. Hydrological Processes, 28(4): 1951-1961.

Schmidt, A. Gibson, J., Santos, I.R., Schubert, M., Tattrie, K., Weiss, H., 2010. The contribution of groundwater discharge to the overall water budget of two typical Boreal lakes in Alberta/Canada estimated from a radon mass balance. Hydrology and Earth System Sciences, 14(1): 79-89.

Shelley, F., Grey, J., Trimmer, M., 2014. Widespread methanotrophic primary production in lowland chalk rivers. Proceedings of the Royal Society B: Biological Sciences, 281(1783): 20132854.

Smith, J., Melville, M.D., 2004. Iron monosulfide formation and oxidation in drain-bottom sediments of an acid sulfate soil environment. Applied Geochemistry, 19(11): 1837-1853.

Smith, J., van Oploo, P., Marston, H., Melville, M.D., Macdonald, B.C.T., 2003. Spatial distribution and management of total actual acidity in an acid sulfate soil environment, McLeods Creek, northeastern NSW, Australia. CATENA, 51(1): 61-79.

Stringer, C.E., Burnett, W.C., 2004. Sample bottle design improvements for radon emanation analysis of natural waters. Health Physics, 87(6): 642-646.

Turetsky, M.R. Kotowska, A., Bubier, J., Dise, N.B., Crill, P., Hornibrook, E.R.C., Minkkinen, K., Moore, T.R., Myers-Smith, I.H., Nykänen, H., Olefeldt, D., Rinne, J., Saarnio, S., Shurpali, N., Tuittila, E.-S., Waddington, J.M., White, J.R., Wickland, K.P., Wilmking, M., 2014. A synthesis of methane emissions from 71 northern, temperate, and subtropical wetlands. Global Change Biology, 20(7): 2183-2197.

Webb, J.R., Maher, D.T., Santos, I.R., 2016. Automated, in situ measurements of dissolved CO_2, CH_4, and $\delta^{13}C$ values using cavity enhanced laser absorption spectrometry: Comparing response times of air-water equilibrators. Limnology and Oceanography: Methods, 14(5): 323-337.

Weiss, R.F., 1974. Carbon dioxide in water and seawater: the solubility of a non-ideal gas. Marine Chemistry, 2(3): 203-215.

Whiticar, M.J., Faber, E., 1986. Methane oxidation in sediment and water column environments—Isotope evidence. Organic Geochemistry, 10(4–6): 759-768.

Whiticar, M.J., 1999. Carbon and hydrogen isotope systematics of bacterial formation and oxidation of methane. Chemical Geology, 161(1–3): 291-314.

Whiting, G., Chanton, J., 1993. Primary production control of methane emission from wetlands.

Wilson, B.P., 1995. Soil and Hydrological relations to drainage from sugarcane on acid sulphate soils, University of New South Wales.

Wilson, B., White, I., Melville, M., 1999. Floodplain hydrology, acid discharge and change in water quality associated with a drained acid sulfate soil. Marine and Freshwater Research, 50(2): 149-157.

Wong, V.N.L. Johnston, S.G., Burton, E.D., Bush, R.T., Sullivan, L.A., Slavich, P.G., 2011. Anthropogenic forcing of estuarine hypoxic events in sub-tropical catchments: Landscape drivers and biogeochemical processes. Science of The Total Environment, 409(24): 5368-5375.

Yamamoto, S., Alcauskas, J.B., Crozier, T.E., 1976. Solubility of methane in distilled water and seawater. Journal of Chemical and Engineering Data, 21(1): 78-80.

Yvon-Durocher, G. Allen, A.P., Bastviken, D., Conrad, R., Gudasz, C., St-Pierre, A., Thanh-Duc, N., del Giorgio, P.A., 2014. Methane fluxes show consistent temperature dependence across microbial to ecosystem scales. Nature, 507(7493): 488-491.

Figure 1: Location of study site and sampling points: (a) McLeods Creek sub-catchment located within the Tweed River floodplain (1,100 km^2), the northern-most coastal region of New South Wales, eastern Australia (from Smith and Melville, 2004); and (b) sub-catchment (0.01 km^2) where the time series was carried-out. The extensive drainage network and the location of discrete groundwater and surface water samples is shown.

Figure 2: Time series of rainfall and hydrology data in the Tweed Valley sugarcane sub-catchment during January 19-31, 2015. The continuous monitoring period January 26-31, 2015 is shown to the right of the dashed line. (A) daily precipitation (mm); (B) depth from surface in outlet drain (black) and groundwater depth from bore near outlet drain (red); (C) hydraulic head (cm) is defined as the difference between groundwater (GW) and drain surface water (SW) depth, where a positive hydraulic head represents groundwater excess (groundwater height exceeds surface water and negative hydraulic head represents surface water excess (surface water height exceeds groundwater); (D) hourly discharge (m^3); (E) cumulative floodplain discharge (black) and rainfall (red) (ML).

Figure 3: Time series of continuously measured parameters within the outlet drain following the flood event (January, 26-31, 2015). Left stack (from top): dissolved radon (dpm L^{-1}); dissolved CO_2 (μM); dissolved CH_4 (nM); δ^{13}C-CH_4 values (‰); molar ratio CH_4:CO_2; hydraulic head (cm) between groundwater (GW) and surface water (SW). Right stack (from top): temperature (°C); pH; conductivity (μS cm^{-1}); dissolved oxygen (%); drain water depth (cm); and discharge (m^3 min^{-1}) controlled by automatic pump. Shaded areas represent dark hours and coloured bars highlight the duration of each phase. Dashed lines represent pre-flood conditions.

Figure 4: Measured dissolved ^{222}Rn (dpm L^{-1}), CO_2 (μM), CH_4 (nM), and δ^{13}C-CH_4 values (‰) as a function of water table position below the soil surface (cm) of bore adjacent to the outlet drain during time series (January, 26-31, 2015).

Figure 5: Conceptual model of the major carbon flux pathways and CO_2 and CH_4 dynamics during the post-flood period within the artificial drains of a modified floodplain. Each numbered box diagram represents a consecutive phase during the recovery of flood to baseline conditions with; 1) being the flood phase; 2) groundwater excess phase; 3) recovery phase; and 4) the phase where baseline conditions are

achieved. Two stacks of box diagrams are provided for CO_2 and CH_4 individually. Coloured arrows represent the different input and outputs of CO_2/CH_4 fluxes and their relative contribution (numbers in bold related to the contribution to the total flux during each phase). Yellow represents evasion, red represents export, blue represents groundwater flux, and green the unaccounted for flux which we have terms in-drain flux (i.e. processes occurring within the drains). Shaded area within the soil profile shows the groundwater table position.

Figure 6: Diurnal CH_4 concentration trends in response to: (A) time of day (hour), and (B) dissolved oxygen concentrations in surface water (% saturation); separated into five days over the continuous monitoring period. Each day is displayed over a 24 h period between 12:00 pm to 12:00 pm. In figure 6A, the time of day was partitioned into periods where methane oxidation dominates (oxidation zone), methane oxidation shifts to methane production (transition zone), and methane production dominates (production zone). The inset in B shows a hysteresis loop that occurred in days 1,2, 3, and 4.
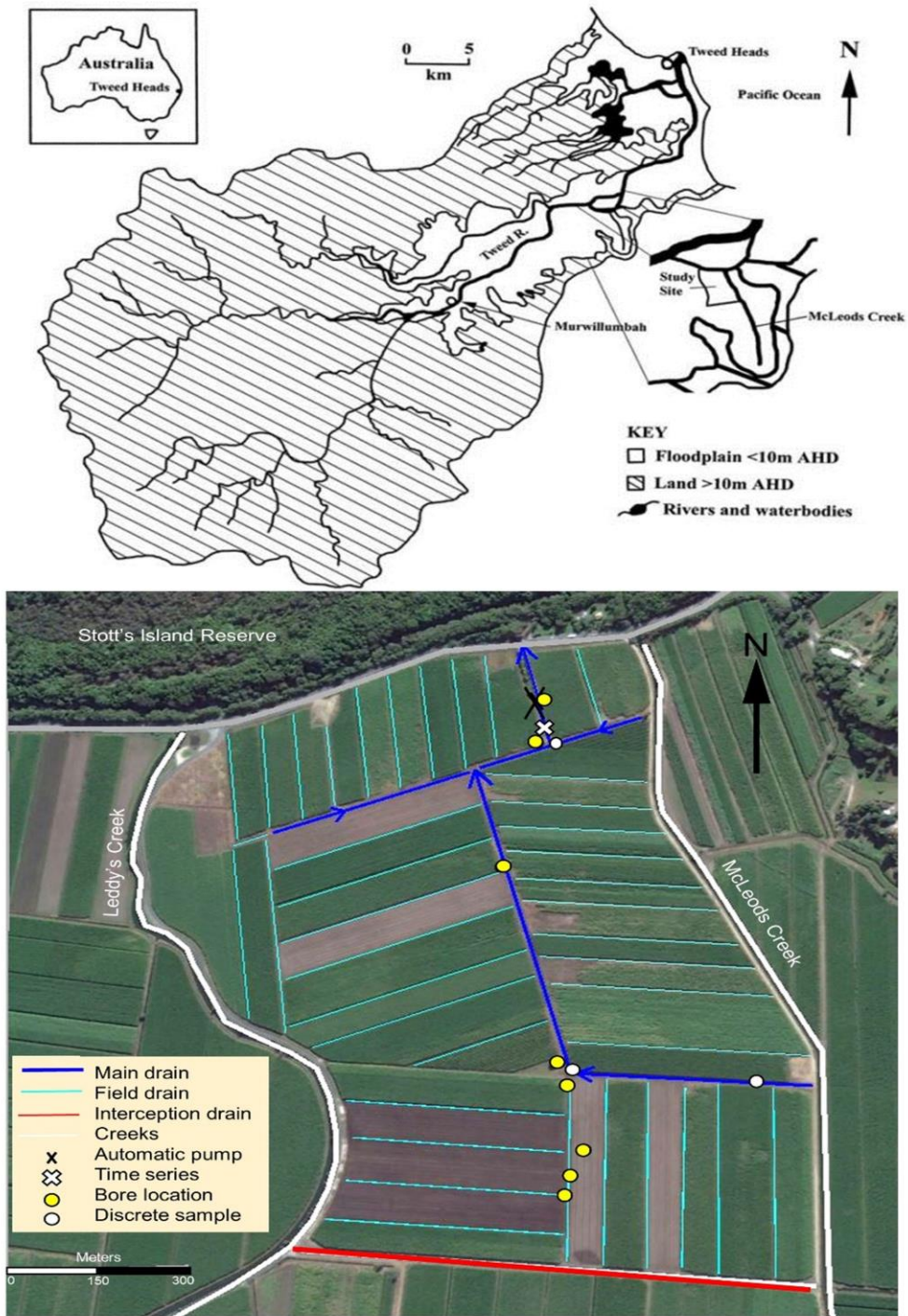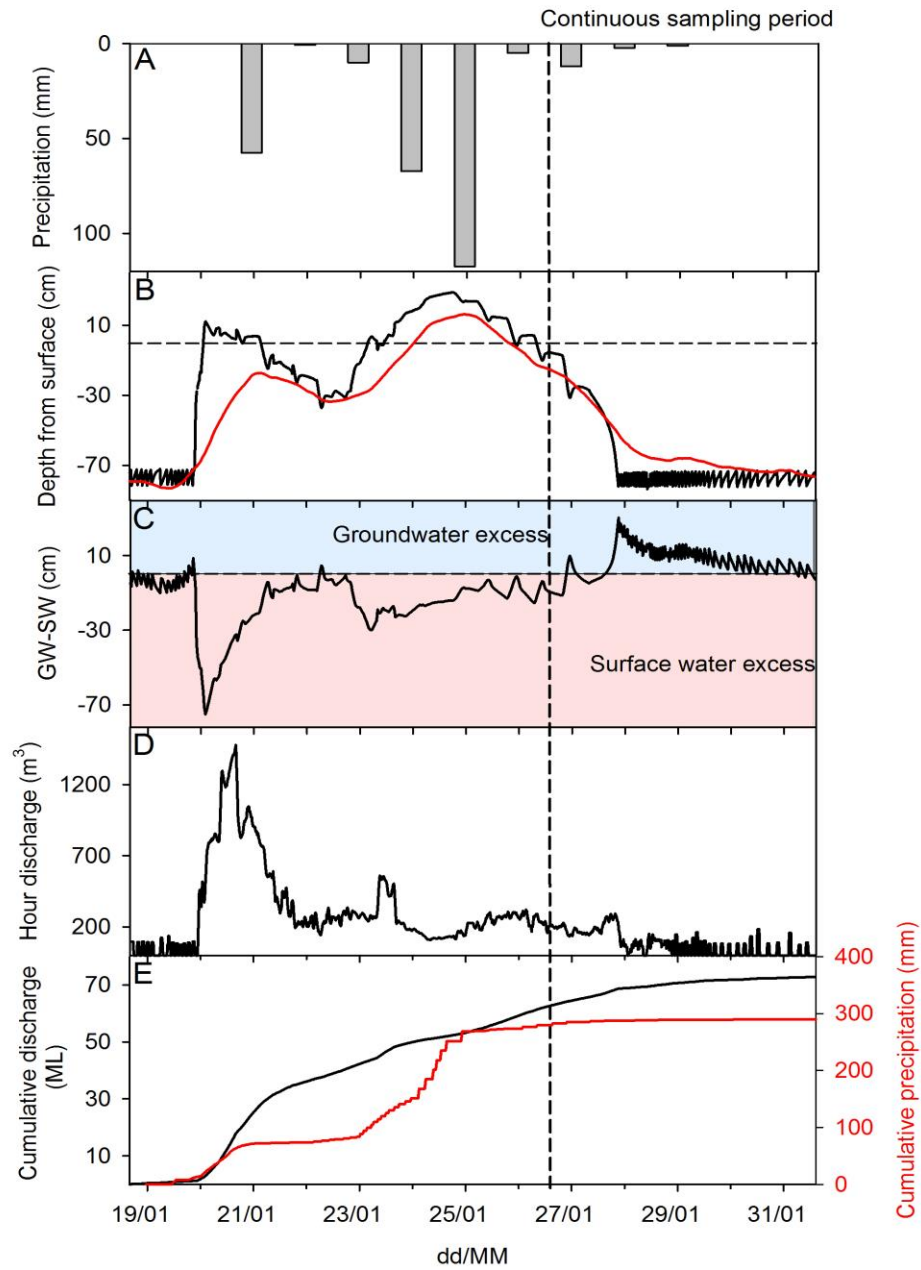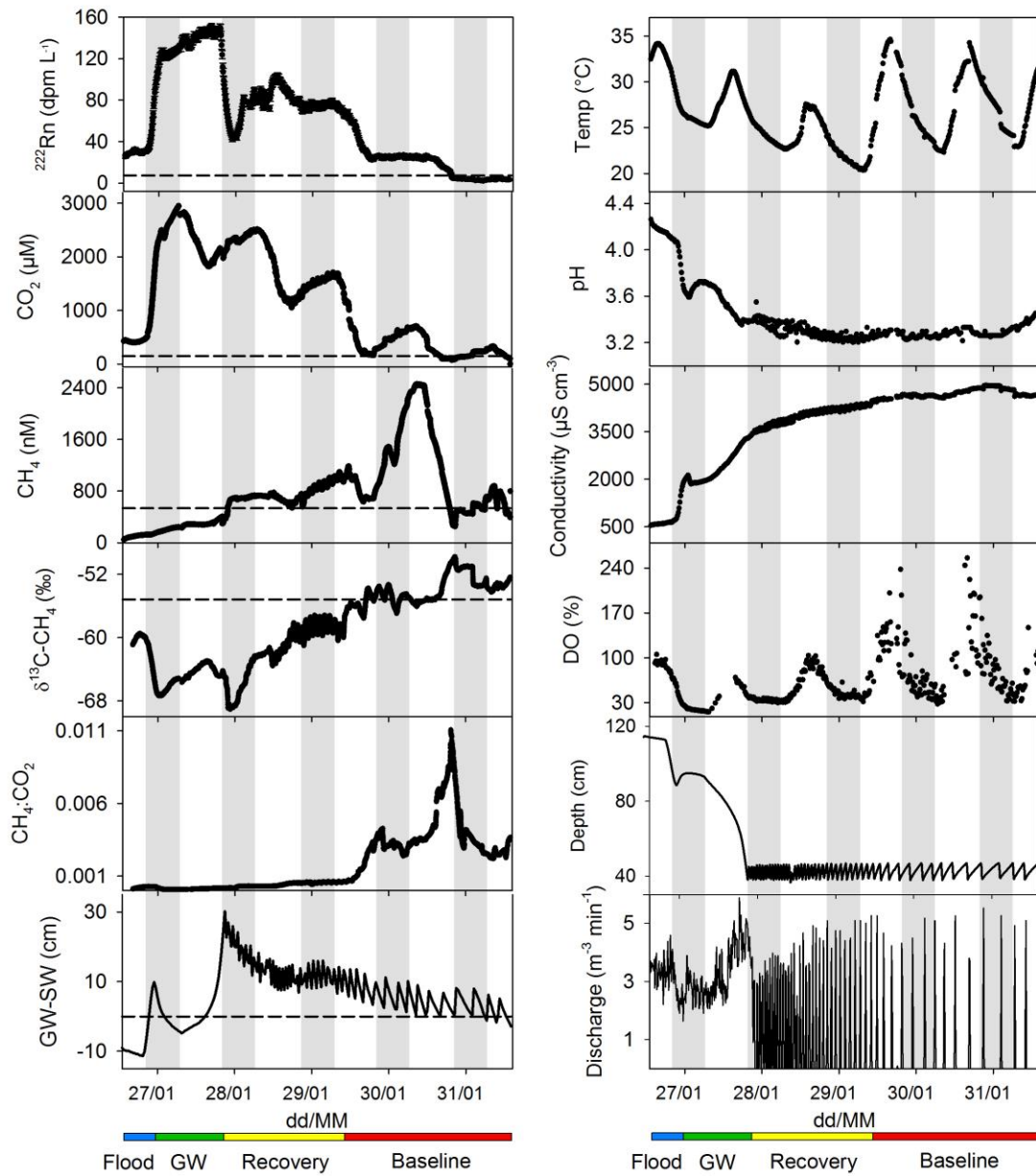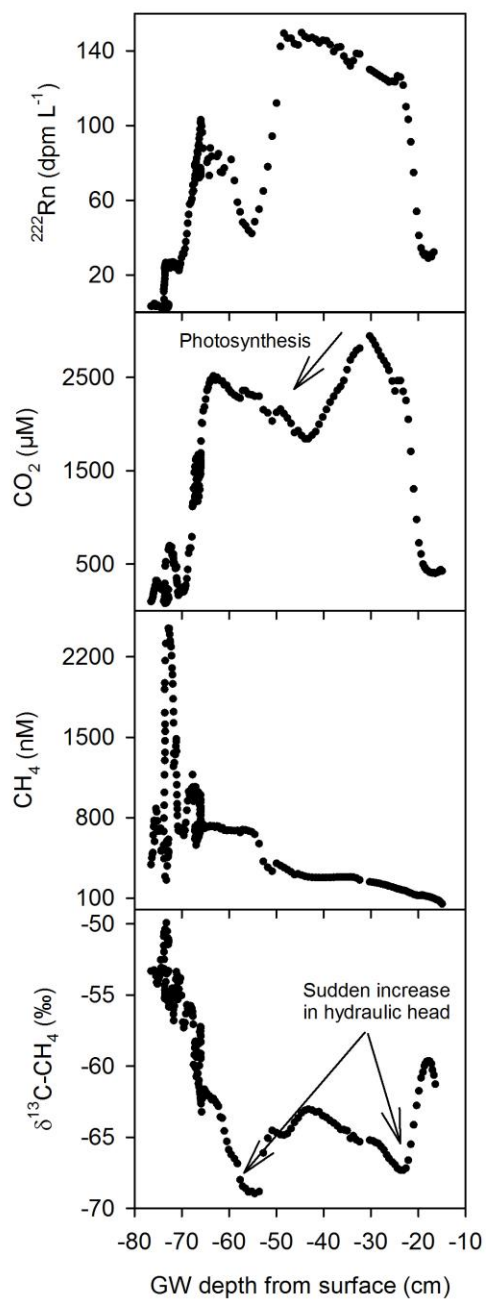
Fig. 1

Fig. 2

Fig. 3

Fig. 4
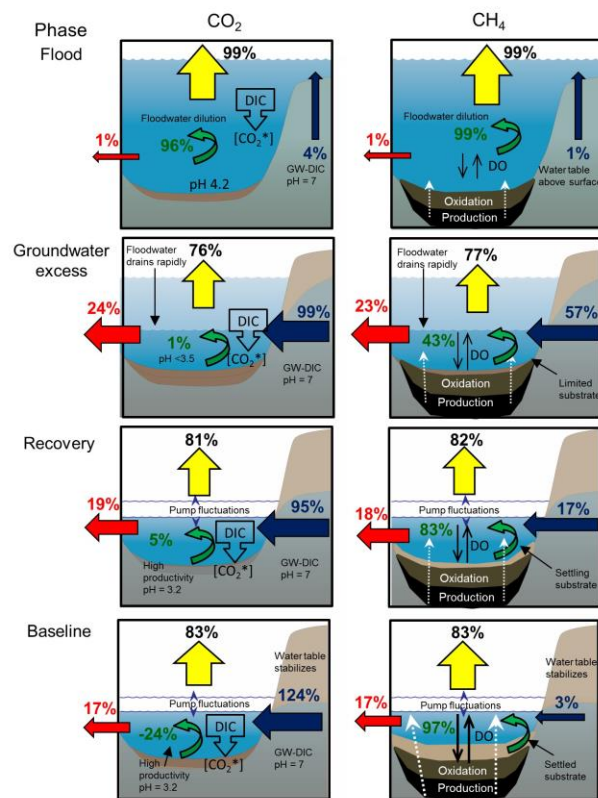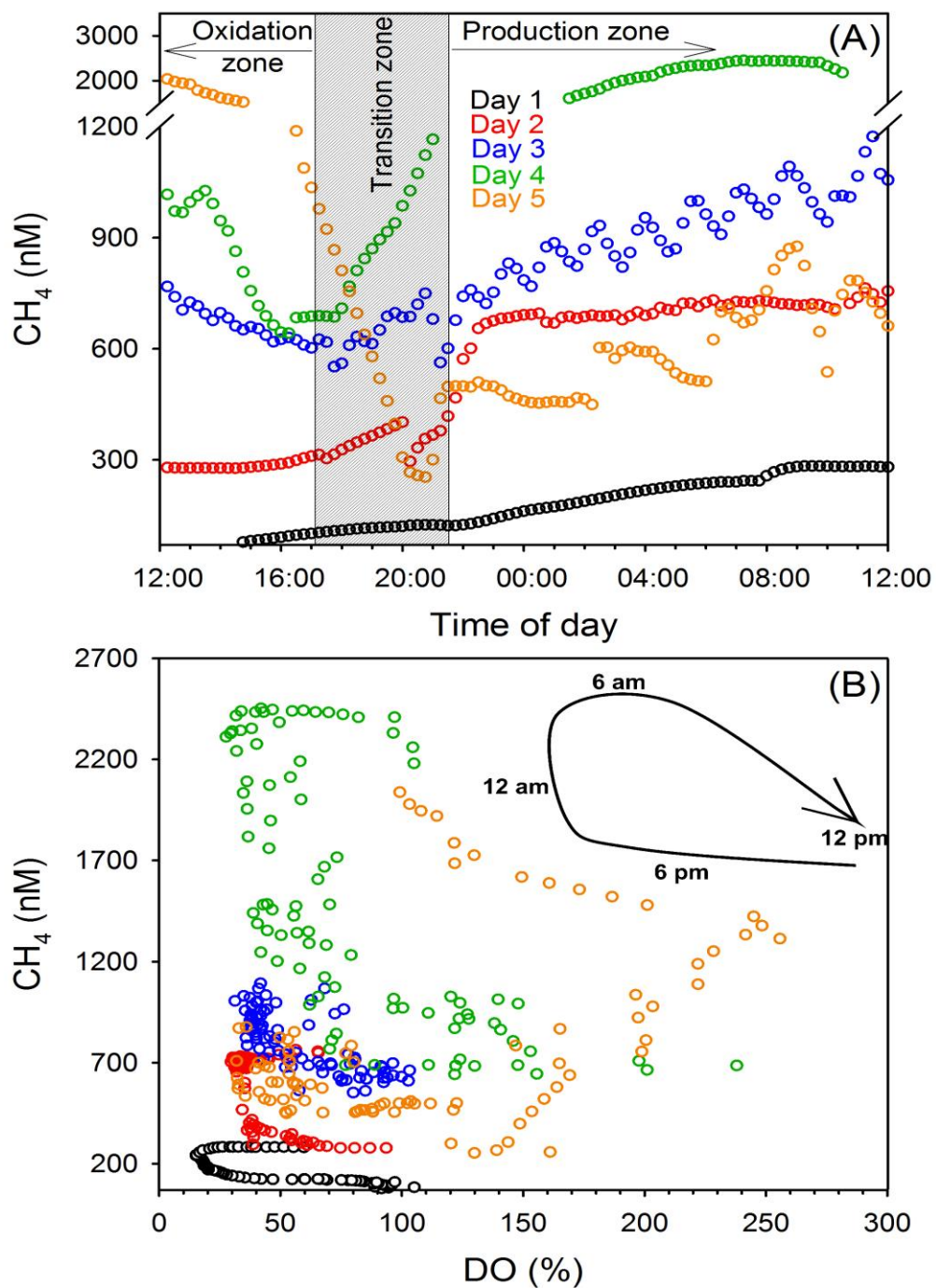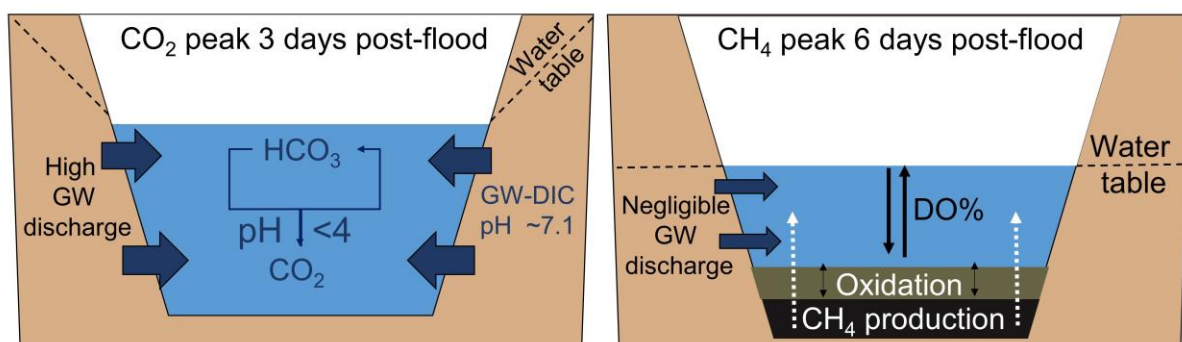
Fig. 5

Fig. 6

Graphical abstract

Table 1: Average ± standard error of measured parameters taken as discrete samples outside of continuous monitoring. Pre-flood represents conditions 5-6 weeks before time series deployment, flood is 1-3 days before time series deployment, and post-flood is 1-4 weeks after time series deployment. Groundwater samples were taken from eight sites within the sub-catchment as shown in Figure 1.

	$[CO_2*]$ (μM)	DIC (μM)	$\delta^{13}C$-CO_2 (‰)	CH_4 (nM)	$\delta^{13}C$-CH_4 (‰)	^{222}Rn (dpm L^{-1})	pH	Conductivity (μS cm^{-1})
Pre-flood	148 ± 31	1,915 ± 442	-9.3 ± 0.8	534 ± 137	-55.2 ± 3.0	7 ± 2	6.75 ± 0.31	43,335 ± 414
Flood	284 ± 64	536 ± 89	-14.9± 1.9	121 ± 53	-53.0 ± 3.2	36 ± 12	4.71 ± 0.24	616 ± 205
Flood recession	1,169 ± 900	1,057 ± 645	-12.8 ± 2.9	765 ± 558	-58.83 ± 4.9	60 ± 45	3.42 ± 0.24	3,724 ± 1,236
Post-flood	223 ± 60	224 ± 51	-15.2 ± 1.3	2,798 ± 156	-47.1 ± 1.8	10 ± 3	3.38 ± 0.12	6,935 ± 617
Groundwater	1,693 ± 495	10,533 ± 1,280	-16.5 ± 1.0	548 ± 185	-66.6 ± 4.9	146 ± 27	7.05 ± 0.22	11,233 ± 1,068

Table 2: Results of radon mass balance calculations for groundwater flux estimates showing averages with the range in parenthesis. Radon sources other than groundwater were assumed to be constant and produce concentrations of 2,400 dpm m^{-3}. Radon loss (^{222}Rn$_{ex}$loss) is the radon flux that needs to be explained by groundwater. The lower and upper limits of the groundwater flux represent the error associated with the ^{222}Rn endmember concentrations (146 ± 27). Total % of discharge is based on the sum of the average groundwater flux over total surface water discharge for each phase.

Phase	Flood (0.25 days)	GW surplus (0.89 days)	Recovery (1.6 days)	Baseline (2.1 days)	Total (5 days)
^{222}Rn$_{ex}$ (dpm m^{-3})	34,400 (26,005-78,147)	131,078 (84,572-147,216)	74,030 (39,714-100,584)	17,127 (57-65,620)	
^{222}Rn$_{ex}$ loss (dpm day^{-1})	1.51E+8 (8.77E+7-2.43E+8)	6.14E+8 (2.49E+8-1.18E+9)	2.30E+8 (1.63E+7-9.79E+8)	2.64E+7 (-2.01E+3 - 5.03E+8)	1.46E+11
$Q_{gw-lower}$ flux (m^3 day^{-1})	871 (505-1,404)	3,540 (1,435-6,851)	1,319 (94-5,644)	150 (-1-2,903)	5,736
$Q_{gw-upper}$ flux (m^3 day^{-1})	1,274 (739-2,053)	5,177 (2,099-10,020)	1,931 (138-8,255)	219 (-2-4,247)	8,389
Q_{gw-av} flux (m^3 day^{-1})	1,034 (600-1,667)	4,204 (1,705-8,138)	1,567 (112-6,704)	178 (-1-3,449)	6,924
Q_{gw-av} flux (cm day^{-1})	0.21 (0.12-13.2)	35.6 (11.3-85.7)	21.2 (1.4-86.6)	2.4 (-0.02-45.8)	
% of surface discharge	22 ± 4	91 ± 15	84 ± 13	29 ± 6	71 ± 13

Table 3: Total fluxes of CO_2 (kg) and CH_4 (g) over each phase from different inputs (groundwater and in-drain sources) and exports (evasion and aquatic export). Total flux represents the final flux exported over the entire study period.

	Flood (0.25 days)	GW surplus (0.89 days)	Recovery (1.6 days)	Baseline (2.1 days)	Total flux (kg)
CO_2 evasion (kg)	$2,982 \pm 40$	$1,348 \pm 95$	985 ± 12	115 ± 1.5	$5,430 \pm 190$
Total CO_2 export (kg)	29 ± 6	419 ± 84	231 ± 46	24 ± 5	703 ± 141
GW [CO_2*] flux (kg)	20 ± 7.1	281 ± 98	186 ± 65	28 ± 10	515 ± 179
GW DIC-CO_2 flux (kg)	126 ± 28	$1,746 \pm 391$	$1,160 \pm 260$	172 ± 38	$3,204 \pm 717$
CH_4 evasion (g)	225 ± 13	61 ± 4	146 ± 8	129 ± 7	560 ± 31
Total CH_4 export (g)	2.3 ± 0.5	18 ± 3.7	33 ± 6.8	26 ± 5.3	79 ± 16
GW CH_4 flux (g)	3.3 ± 1.1	45 ± 15	30 ± 10	4.4 ± 1.5	89 ± 27
In-drain CO_2 (kg)	$2,884 \pm 50$	22 ± 410	56 ± 235	-33 ± 45	$2,929 \pm 755$
In-drain CH_4 (g)	224 ± 13	34 ± 16	149 ± 15	150 ± 9	556 ± 45

Evasion flux estimates were calculated using O'Connor and Dobbins (1958) k equation using velocity and depth and Ho et al. (1997) k_{600} value of 0.93 cm h^{-1} to calculate the diffusive fluxes during periods of no flow. Groundwater-derived CO_2 and CH_4 fluxes are calculated from the average groundwater flux estimated by the radon mass balance calculations. GW-[CO_2*] refers to groundwater-derived fluxes calculated from the free CO_2 endmember, and DIC-CO_2 refers to calculations using measured total alkalinity converted to DIC that is seen as the 'potential CO_2' endmember when discharging into acidic surface waters. In-drains sources = (Average evasion + export) – GW flux.

Highlights

- Opposing response of dissolved CO_2 and CH_4 concentrations post-flood

- Post-flood peaks of 2,950 μM for CO_2 and 2,400 nM for CH_4

- Groundwater discharge sustained CO_2 evasion via acidification of DIC

- Post-flood conditions enhanced diel oscillations in CH_4

- Drainage canals were a significant source of CO_2 and CH_4 following a flood